applied optics

Demonstration of vacuum strain effects on a light-collection lens used in optical polarimetry

K. W. Trantham,[1,*] K. D. Foreman,[2] and T. J. Gay[2]

[1]University of Nebraska—Kearney, Kearney, Nebraska 68849, USA
[2]University of Nebraska—Lincoln, Lincoln, Nebraska 68588, USA
*Corresponding author: tranthamkw@unk.edu

Received 12 December 2019; revised 5 February 2020; accepted 5 February 2020; posted 10 February 2020 (Doc. ID 385004); published 12 March 2020

The precision by which an electron spin polarization measurement can be made using a noble-gas polarimeter depends directly on the accuracy of a light-polarization measurement. Since the electron–noble gas collisions occur in a vacuum chamber and the optical polarimeter is generally outside the chamber, this work examines the effect the vacuum window has on the perceived optical polarization. A model light source, lens system, and optical polarimeter are used that approximate the situation found in a typical atomic physics experiment. It was demonstrated that a pressure difference of 1 atm on a lens will alter the perceived polarization by as much as 0.05% with typical borosilicate (BK) lenses. This effect was demonstrated to scale with the thickness of the lens used and changes signs when the direction of the stress is reversed.

https://doi.org/10.1364/AO.385004

1. INTRODUCTION

In the service of third-generation parity violation experiments at the Thomas Jefferson National Laboratory and the Mainz Microtron, efforts are underway to make measurements of electron polarization at the injectors for these facilities using megaelectron volt Mott polarimetry to an *accuracy* of ~0.5% [1]. Ultimately, Mott polarimetry requires a theoretical calculation of the Sherman function—the elastic, single-target-atom-scattering analyzing power of the measurement—to put the final experimental asymmetry on an absolute scale [2]. The accuracy of these calculations in the 5 MeV range can probably be done at the 0.5% level for the basic scattering process, but the effect on overall accuracy of the inclusion of radiative corrections and bremsstrahlung in the calculation has yet to be assessed in detail [3]. Thus, a conservative estimate at present of the accuracy with which we can know such Sherman functions is perhaps 1%, yielding an overall accuracy of megaelectron volt Mott measurements at about the same level. In order to achieve a Mott measurement with an accuracy of 0.5%, an independent calibration with this level of accuracy will be required. One option for such a calibration involves the technique of accurate electron spin optical polarimetry (AESOP) [4].

Using atomic fluorescence polarization to measure electron polarization was first proposed formally in 1969 by Farago and Wykes [5,6]. They suggested the use of Zn or Hg targets. Subsequently, Gay *et al.* showed that any of the noble gases could be used instead [7]. The basic idea is simple: the polarized electrons to be analyzed excite atoms through an exchange reaction. Their spin is converted, in part, to orbital orientation by spin-orbit coupling in the excited target state. Upon decay of this state, the fluorescence polarization can be connected kinematically (i.e., without resort to a dynamical calculation) to P_e:

$$P_e = \frac{S/I}{a + b(M/I)}, \tag{1}$$

where a and b are determined by simple angular momentum coupling algebra, and M/I and S/I are the relative Stokes parameters corresponding to linearly polarized light (referenced to the incident electron beam axis) and to circularly polarized light, respectively [8]. Kinematic determination of a and b requires that the excited atom be in a Russel-Saunders state. In this case, the third Stokes parameter, C/I, which is the linear polarization fraction referenced at 45°/135° to the beam axis, must be identically zero [9]. Thus, the measurement of S/I essentially determines P_e, the measurement of M/I determines the polarimeter's analyzing power, and a null check of C/I establishes the validity of the method. Figure 1 shows a typical optical polarimeter geometry.

The optical method has a number of important advantages, its chief one being that it is absolute. It also has higher analyzing power than, e.g., Mott scattering, varying from about 50% for He targets to 70% for heavy noble gases. The main disadvantages of electron optical polarimeters are that they are inefficient and require low energy input beams. Typically, tens of nanoamperes of beam are required to ensure measurement times

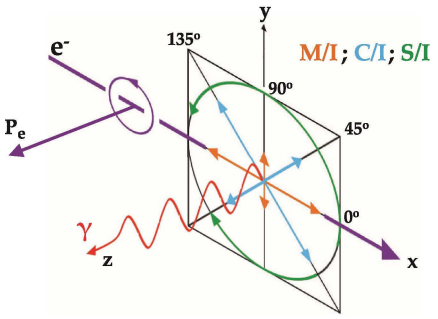

Fig. 1. Typical geometry for electron optical polarimetry. Electrons having transverse polarization along the z axis are incident on the target along the x axis. Fluorescence is best detected along the direction of the electron spin. The relative Stokes parameters of the fluorescence are indicated schematically in the $x-y$ plane with green arrows (circular polarization S/I), blue arrows (canted linear polarization C/I), and orange arrows (linear polarization M/I).

<10 min. Incident energies must correspond to those associated with atomic valence shell excitation, namely, 10–20 eV.

In order to calibrate a Mott polarimeter to 0.5%, and assuming a Mott measurement precision of 0.3% (which is feasible at megaelectron volt energies), an electron beam must be delivered to the Mott analyzer with a polarization that is known absolutely to 0.4%. The current best values for systematic and statistical uncertainty for an optical measurement of electron polarization were obtained two decades ago by our group using an early prototype of an AESOP polarimeter [10]. We were able to obtain a statistical accuracy of 0.5% using a Kr target and, separately, estimated the systematic uncertainty in a similar measurement made with He to be 0.8%. The former measurement was made with a particularly inefficient polarimeter over the course of a few hours. With a polarimeter we have recently demonstrated, a P_e of, e.g., 20% can be measured to 0.2% of itself in 13 s with 1 μA of current [11]. We are confident that a thorough effort to eliminate potential systematic error can achieve the requisite accuracy of 0.4%.

One crucial issue in determining the ultimate accuracy of the AESOP method is the effect that lenses used to collect the light from the excited atomic target have on the polarization of the fluorescence. Since the electron–noble gas collisions occur in a vacuum chamber, and the optical polarimeter is generally at atmosphere outside the chamber, the question arises: what effect does the vacuum window have on the perceived optical polarization and how does this limit the accuracy with which P_e may be measured? A related question is: how do the optical polarimetric properties of a window (its linear dichroism or retardance) change as a result of the mechanical stress caused by a 1 atm pressure difference across it?

Changes in the index of refraction of vacuum windows have been observed [12] to be as large as 1 part in 10^8. It is possible to compensate for stress-induced birefringence in some applications [13]. However, the situations discussed in Refs. [12,13] involve a spatially narrow beam of light that traverses a small portion of the optical element. The statistical precision of noble gas electron polarimetry is generally limited by low light intensity. Thus, maximizing the solid angle of emission subtended by the detector can be important, which in turn means that large fractions of the polarimetric optical elements must be illuminated.

Since this requires a light-collection and collimation lens in addition to a vacuum window, a single lens can serve in both capacities. This reduces the total number of interfaces that could potentially alter the polarization observed. It is possible to monitor and correct for birefringence in a lens using a sectored liquid–crystal retarder [14], but again, this requires more light than is typically available from atomic fluorescence and would be difficult to implement *in situ* with a polarimeter. Thus, the focus of the present investigation is to understand the changes in optical polarization produced by a combination lens/vacuum barrier, which is largely illuminated by the polarized light when stressed with pressure differences on the order of 1 atm. Of course, another option would be to avoid an optical vacuum interface entirely by building a polarimeter that can operate *in vacuo*. This approach has both advantages and disadvantages, the latter having primarily to do with heat dissipation and thermal effects on the optical elements that can become important in high-accuracy measurements. In a parallel effort, we have largely solved these problems and have used a polarimeter capable of vacuum operation to make the measurements reported here. This polarimeter will be discussed in a future publication [15]; here we provide only a general description of its construction.

2. APPARATUS

In this investigation, the three key components of the apparatus are: (1) a source of strongly polarized light, (2) a combination light-collimating compound lens and vacuum barrier, and (3) an optical polarimeter to measure the resulting polarization after passing through the lens. Referring to Figure 2, the polarized light source consists of a light-emitting diode (LED) (labeled as "A"), a high-contrast "glass" linear polarizer (Edmund #47-316) ("B"), and a 2 mm aperture ("C"). These components are mounted coaxially in a Conflat reducing nipple (Ideal Vacuum Products #P104736). The mounting hardware supporting the LED, polarizer, and aperture has large venting holes so that the chamber can be quickly pumped to vacuum or pressurized as needed.

The collimating lens system ("D") serves as a pressure barrier separating the light source and polarimeter chamber. Two different double-lens chambers are used to see if any pressure-related polarization effects depend on lens thickness. The first system uses two 50 mm diameter borosilicate (BK) plano–convex lenses (Edmund Stock #32-974), each with a nominal focal length of 150 mm and center thickness $CT = 9.0$ mm, installed with the flat sides facing each other. The two lenses are mounted in a double-sided Conflat flange (Ideal Vacuum Products #P105835) with vacuum-compatible epoxy such that there is a small void separating the two lenses. A port is bored radially through the flange, permitting pressure control of this space between the lenses.

The second collimating lens chamber used in this study also uses two plano–convex lenses, similarly installed with their flat sides facing each other. However, these lenses are thinner (Thorlabs LA1725) with focal lengths $f = 400$ mm and center thickness $CT = 4.6$ mm. This second system is identified as

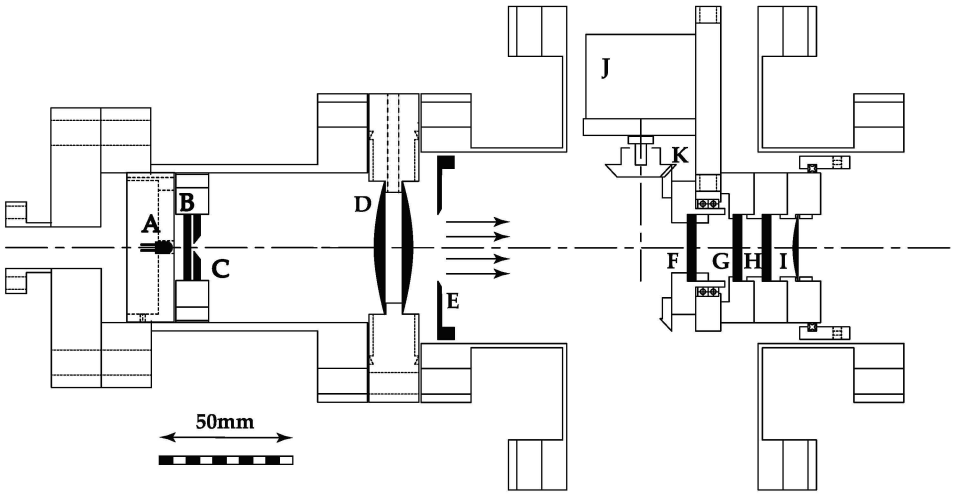

Fig. 2. Apparatus diagram illustrating key components. See text for item descriptions. The polarimeter chamber uses a Conflat four-way cross (Ideal Vacuum Products #P104691).

the "thin" system. Rather than replacing the light-source vacuum chamber to accommodate the longer effective focal length, another lens (Edmund Stock #45-227 $f = 5.0$ mm) is placed immediately in front of the LED to produce a virtual image at ~200 mm from the thin double-lens chamber. When the light source is assembled with either lens system, the output light through the polarimeter is checked for accurate collimation.

The polarimeter consists of the necessary optical components to measure the Stokes parameters of light transmitted through the lenses. A full description of the optics and the procedure for measuring optical polarization is given below. Briefly (Fig. 2), the polarimeter consists of a 25 mm diameter entrance aperture ("E") blackened with colloidal graphite, a rotatable multiple-order quartz retarder (Edmund #43-698; "F"), a high-contrast "glass" linear polarizer (Edmund #47-316; "G"), a 656 ± 10 nm (Hα) bandpass filter (Edmund #65-716; "H"), and a 175 mm focal-length refocusing lens ("I"). All optics have a 20 mm clear aperture, and the interior of the polarimeter is blackened with colloidal graphite. A stepper-motor ("J") and bevel gear system ("K") are used to rotate the retarder. All of the above components are mounted in a four-way Conflat cross (Ideal Vacuum Products #P104691) so that the polarimeter chamber may be evacuated or pressurized as needed. Light traversing the polarimeter optics exits through a BK-7 glass vacuum window and is detected with a Hamamatsu 1P28 photomultiplier, not shown.

3. POLARIMETRY

The Stokes parameters of the light are measured following a standard method [16]. The light propagation defines the $+z$ axis, which is coaxial with the optical system, as in Fig. 3. The retarder is assumed to have retardance δ, and its fast axis is initially at some angle β_0 relative to an arbitrary x axis. The transmission axis of the linear polarizer is fixed at angle α, also relative to the x axis. The light transmitted through the optical system as a function of retarder angle β is thus given by

$$\begin{aligned} I_T(\alpha, \beta, \delta) = \frac{1}{2}\left[I + \left(\frac{M}{2}\cos 2\alpha + \frac{C}{2}\sin 2\alpha\right)(1+\cos\delta)\right] \\ + \frac{1}{2}\left[S \sin\delta \sin(2\alpha - 2\beta + 2\beta_0)\right] \\ + \frac{1}{4}\left[(M\cos 2\alpha - C\sin 2\alpha)\cos(4\beta - 4\beta_0)\right. \\ \left. + (M\sin 2\alpha + C\cos 2\alpha)\sin(4\beta - 4\beta_0)\right] \\ \times (1-\cos\delta), \end{aligned} \tag{2}$$

where I, M, C, and S are the standard Stokes parameters.

Equation (2) is essentially a finite Fourier sum. Expressed with discrete coefficients, this becomes

$$\begin{aligned} I_T(\alpha, \beta, \delta) = C_0 + C_2\cos 2\beta + S_2 \sin 2\beta \\ + C_4\cos 4\beta + S_4 \sin 4\beta. \end{aligned} \tag{3}$$

For a single polarization measurement, values of the transmitted light $I_T(\beta_i)$ are recorded as the retarder is rotated through one revolution in increments of $\Delta\beta$. For an even number, $N = 2L$, of $I_T(\beta_i)$ values in a trial, the coefficients are

$$C_k = \frac{2}{N}\frac{1}{1+\delta_{k0}+\delta_{kL}}\sum_{i=0}^{N-1} I_{Ti}\cos(\omega_k\beta_i) \tag{4}$$

and

$$S_k = \frac{2}{N}\frac{1}{1+\delta_{k0}+\delta_{kL}}\sum_{i=0}^{N-1} I_{Ti}\sin(\omega_k\beta_i), \tag{5}$$

with $\omega_k = \frac{2\pi}{N}\frac{k}{\Delta\beta}$ and $\beta_I = i\cdot\Delta\beta$. Once the Fourier coefficients are determined, the relative Stokes parameters M/I, C/I, and S/I can be determined from Eqs. (2) and (3) (see also Ref. [17]). A representative polarization measurement is shown in Fig. 4.

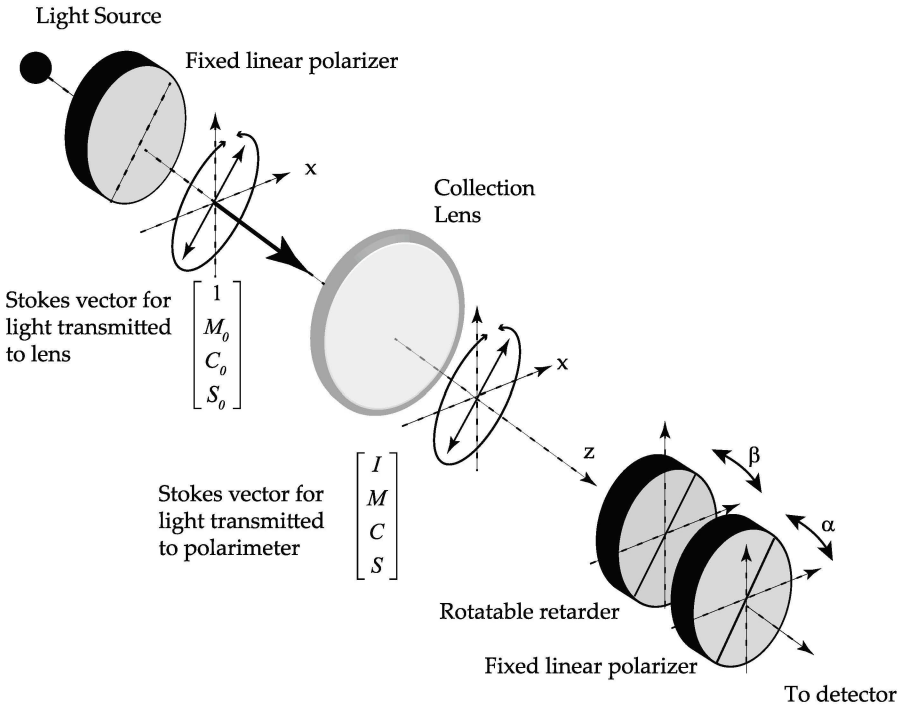

Fig. 3. Geometry of the optical polarimeter.

Since we are concerned with, among other things, possible stress-induced birefringence in the lens, it is useful to estimate what one might expect. First, the lens is modeled as a retarder with some pressure-dependent retardance δ' with its fast axis at angle β'. Then, we assume that the input light polarization is elliptical with Stokes vector $[1, M_0, C_0 = 0, S_0]$. Although we have set the Stokes parameter C_0 equal to zero, generality is not lost, since β' is variable. The output Stokes vector transmitted and observed by the polarimeter is given by

$$\begin{bmatrix} I \\ M \\ C \\ S \end{bmatrix} = \begin{bmatrix} 1 & 0 & 0 & 0 \\ 0 & \cos^2 2\beta' + \cos\delta' \sin^2 2\beta' & \sin 2\beta' \cos 2\beta' \left(1 - \cos\delta'\right) & -\sin 2\beta' \sin\delta' \\ 0 & \sin 2\beta' \cos 2\beta' \left(1 - \cos\delta'\right) & \sin^2 2\beta' + \cos^2 2\beta' \cos\delta' & \cos 2\beta' \sin\delta' \\ 0 & \sin 2\beta' \sin\delta' & -\cos 2\beta' \sin\delta' & \cos\delta' \end{bmatrix} \begin{bmatrix} 1 \\ M_0 \\ 0 \\ S_0 \end{bmatrix}$$

$$= \begin{bmatrix} 1 \\ M_0 \left(\cos^2 2\beta' + \cos\delta' \sin^2 2\beta'\right) - S_0 \sin 2\delta' \sin\delta' \\ M_0 \left(\cos 2\beta' \sin 2\beta' - \cos 2\beta' \cos\delta' \sin 2\beta'\right) + S_0 \cos 2\beta' \sin\delta' \\ S_0 \cos\delta' + M_0 \sin 2\beta' \sin\delta' \end{bmatrix}. \quad (6)$$

To determine under what conditions the experiment will be most sensitive to small changes in lens retardance, the derivative of Eq. (6) is taken with respect to δ', yielding

$$\frac{d}{d\delta'} \begin{bmatrix} I \\ M \\ C \\ S \end{bmatrix} = \begin{bmatrix} 0 \\ -S_0 \sin(2\beta') \\ S_0 \cos(2\beta') \\ M_0 \sin(2\beta') \end{bmatrix}, \quad (7)$$

assuming that δ' is small. Equation (7) suggests that if strongly linearly polarized light is input to the lens, the largest change in polarization is expected to be that of S/I, the relative Stokes parameter corresponding to circularly polarized light.

4. DATA ACQUISITION

A computer-controlled valve manifold is used to set the pressure in the double-lens chamber to some pressure P between 1600 and 0 Torr. Data collection proceeds by measuring the light polarization (e.g., Fig. 4), at two different pressures, repeated many times while holding the pressure in the light source and polarimeter chambers constant. A representative data collection session is given in Fig. 5. The solid line illustrates the pressure in the double-lens chamber in which the pressure is toggled between $P = 1600$ Torr and atmospheric pressure. In the specific example of Fig. 5, the light source and polarimeter chambers were held at atmospheric pressure (~800 Torr). Light polarization is measured 25 times each time a new pressure is established. In the data of Fig. 6, there are a total of 400 polarization measurements at each pressure. Before data are collected at each new pressure, the data-acquisition computer checks the position of the retarder by advancing the motor by a known number of steps, then finding home again. The number of steps required to find home at each set of pressures is logged to a data file.

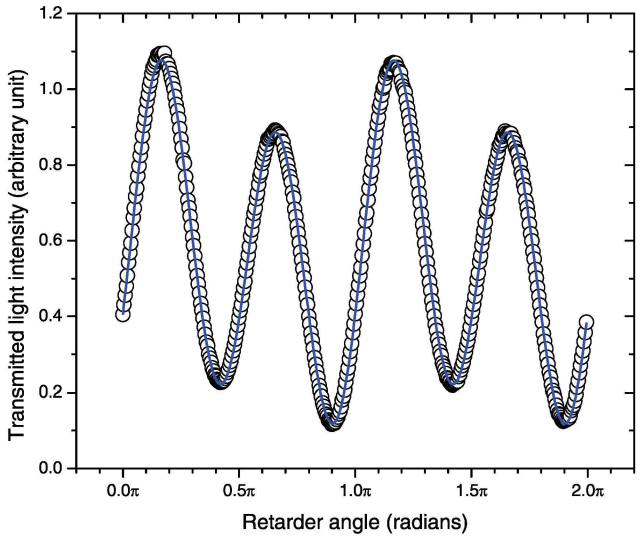

Fig. 4. Representative polarization measurements (open circles) and fit (solid line) according to Eqs. (2) and (3), giving $M/I = -0.432$, $C/I = 0.888$, and $S/I = 0.156$ with an $R^2 = 0.9997$ for the fit. Data reduction and error estimation are discussed in the text.

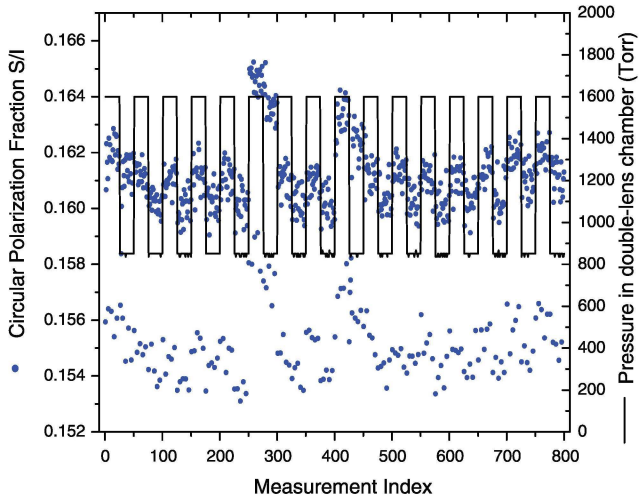

Fig. 5. Example data showing circular polarization fraction (S/I) measured as the pressure in the double lens is toggled between $P = 1600$ Torr and atmosphere (~800 Torr). In this example, the pressure in the light source and polarimeter is held constant at atmospheric pressure. The stray data between measurement indices 240 and 450 are discussed in the text.

The solid circles in Fig. 5 show the measured circular polarization as the pressure in the double-lens chamber is toggled. The data show two groupings of S/I data around $S/I \sim 0.161$ and around $S/I \sim 0.155$. This apparently random change in S/I is believed to be caused by the LED changing its spectral distribution, in the same manner that an unstabilized diode laser mode "hops." Given that the retardance δ of the multiple-order quartz retarder is strongly wavelength-dependent, a small change in LED spectral distribution will yield a different measured polarization. Unfortunately, these random fluctuations are uncontrollable and serve to increase the standard error in the final results. These data are not excluded, on the premise that if

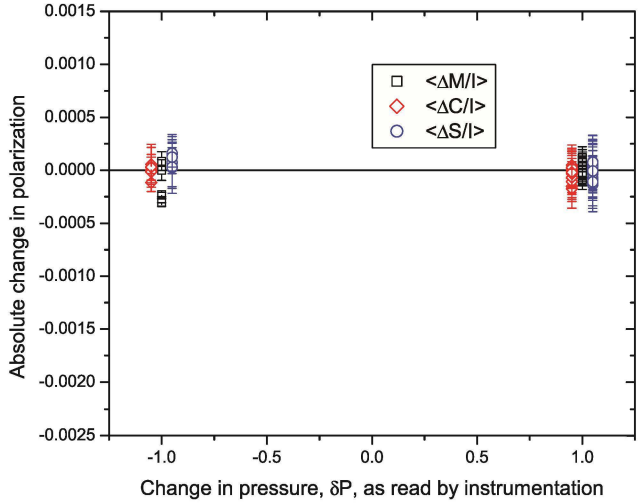

Fig. 6. Estimation of systematic effects; observed polarization changes as the pressure in the valve chamber is toggled per Eq. (8) and recorded by instrumentation. The actual pressure in the lens chamber is held at atmosphere.

the pressure-induced stress of the lens is changing polarization, there will subsequently be correlated changes in polarization, independent of the "mode" in which the LED is operating. Another problem in the data is also apparent near measurement indices 275 and 400. This happens infrequently and is caused by a "homing error" of one step of the motor used to rotate the retarder. The computer will rehome the stepper motor after every pressure-atmosphere toggle to ensure that the retarder is in the correct position. The angular resolution of the motor and homing detection system is 1/400 revolutions, so occasionally the retarder is placed one step from the nominal home position. Since the homing algorithm logs the number of steps at each pressure cycle, it is known when this happens and these data are excluded from further analysis.

It is apparent, particularly for measurement indices greater than 500, that S/I changes synchronously with the pressure in the double-lens chamber. In an effort to mitigate long-term drift effects and to make comparisons with data taken at other pressures, the *difference* in polarization values is reported. Using the data in Fig. 5 as an example, we compute the average circular polarization at 800 Torr ($\langle S/I\rangle_{800,i}$) and 1600 Torr ($\langle S/I\rangle_{1600,i}$) for the ith toggle set, with uncertainties determined from the standard error of the mean for the 25 measurements in each subset. From this, a change in polarization $\Delta S/I_i = \langle S/I\rangle_{800,i} - \langle S/I\rangle_{1600,i}$ is calculated for the ith toggle set, with the uncertainty in $\Delta S/I_i$ determined by adding the uncertainty in $\langle S/I\rangle_{800,i}$ and $\langle S/I\rangle_{1600,i}$ in quadrature. There are 16 sets of pressure changes represented in Fig. 5, so i ranges from 1 to 16. The average of changes (as opposed to the change in averages) is computed $\langle \Delta S/I\rangle = \Sigma\, \Delta S/I_i/16$ with the uncertainty determined by adding individual errors of $\Delta S/I_i$ in quadrature. Using the example data, and excluding the aforementioned "homing error" data, this second approach yields $\langle \Delta S/I\rangle = -1.00(19) \times 10^{-3}$.

Since the pressure in the light source, lens chamber, and polarimeter can be independently controlled, one can produce different combinations of vacuum and/or pressure providing

different magnitudes and directions of stress on the lenses. In the present discussion, only combinations of pressures involving rough vacuum (~0 Torr), atmosphere (~800 Torr), and pressurized air (~1600 Torr) will be considered. Further, the light source and polarimeter chamber will be held at the same pressure during any given experiment. This will keep the magnitude of stress on each half of the lens chamber the same. On occasions in which the polarimeter was under vacuum, a small temperature correction was applied to the data to account for the heating of the retarder by the stepper motor [15].

Our results are reported as the absolute change in polarization relative to that measured with atmosphere in the double lens as a function of the change in stress that the lens experienced during the data set. Recall from Fig. 5 that a data set consists of toggling the pressure in the lens between atmosphere and either vacuum or pressurized air. We define these two pressures in the toggle sequence as P_1 and P_2, respectively, so P_1 is always 1 atm, and P_2 is either 0 or 2 atm. The change in pressure for the data run δP in units of atmospheres is defined as the pressure difference the lens experiences when the double lens is at atmosphere minus the pressure difference the lens experiences when the double lens is at some pressure P_2. Defining the pressure in the polarimeter chamber and source chamber as P, which remains constant during a data set, the change in pressure for a toggle data set becomes

$$\begin{aligned}\delta P &= \Delta P_{\text{atmophere}} - \Delta P_{\text{pressure}} \\ &= (P - P_1) - (P - P_2) = P_2 - P_1. \end{aligned} \tag{8}$$

Thus, the change in pressure for a data run is reported as $\delta P = +1$ atm or $\delta P = -1$ atm, corresponding to $P_2 = 2$ atm or $P_2 = 0$ atm, respectively.

To estimate systematic errors introduced by the data-analysis procedure or by the apparatus, the valve manifold is occasionally removed from the lens chamber. It is sealed with all instrumentation attached, and data are acquired following the same procedure. While the pressure in the valve manifold is toggled and recorded, the actual pressure to the lens chamber never changes and is held at atmosphere. Figure 6 shows typical changes in polarization observed when the system is checked for systematic effects. From this, we conclude that random systematic uncertainties are less than ~0.0002 and that any nonzero changes in polarization greater than this will be caused by actual stresses on the lens.

Many data sets were collected and analyzed in a manner similar to that discussed with regard to Fig. 5. All results are presented in Fig. 7, showing the absolute change in polarization as a function of the pressure difference δP. Each data point is the "average of changes" (e.g., $\langle \Delta S/I \rangle$ and not $\Delta \langle S/I \rangle$), as discussed above for any given trial. Although δP [Eq. (8)] does not depend on the polarimeter and source chamber pressure P, Fig. 7 represents data that have been acquired with P equal to 0, 800, and 1600 Torr. Data from both the "thick" ($CT = 9.0$ mm) lenses and "thin" ($CT = 4.6$ mm) lenses are presented in Fig. 7. For the thick lens data, the input polarization to the system is $M/I = -0.436(1)$, $C/I = 0.882(1)$, and $S/I = 0.152(1)$, determined by averaging all polarizations observed under all pressure conditions. Likewise, the input polarization to the thin lens data is $M/I = 0.975(5)$, $C/I = 0.075(3)$, and $S/I = 0.159(3)$.

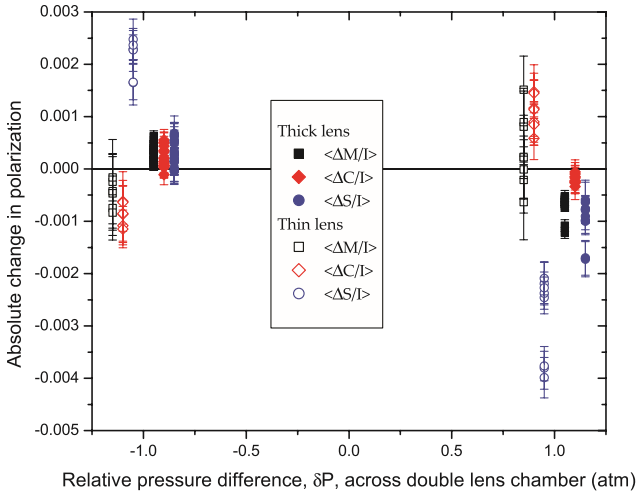

Fig. 7. Change in optical polarization observed as the double-lens chamber is stressed with a variety of pressure differences as defined by Eq. (8). All data occur at $\delta P = \pm 1$, but are shifted on the abscissa to aid in readability.

Table 1. Summary of the Change in Optical Polarization as the Light-Collection Lenses Are Stressed[a]

Lenses	δP	$\langle \Delta M/I \rangle$	$\langle \Delta C/I \rangle$	$\langle \Delta S/I \rangle$
Thick	−1	$2.8(2) \times 10^{-4}$	$2.2(5) \times 10^{-4}$	$2.7(6) \times 10^{-4}$
Thick	+1	$-7.4(4) \times 10^{-4}$	$-2.0(7) \times 10^{-4}$	$-1.0(1) \times 10^{-3}$
Thin	−1	$-5(2) \times 10^{-4}$	$-9(2) \times 10^{-4}$	$2.2(1) \times 10^{-3}$
Thin	+1	$3(2) \times 10^{-4}$	$1.0(2) \times 10^{-3}$	$-2.8(1) \times 10^{-3}$

[a]Data are the weighted average of data presented in Fig. 8.

The average, absolute change in polarization caused by changes in stress on the lens is determined by computing a weighted average of the multiple trials shown in Fig. 7 for each lens. The data are weighted by the standard error of each measurement set (see, e.g., Eq. (7.10) of Ref. [18]). These weighted averages are summarized in Table 1. As suggested by Eq. (7), with strongly linearly polarized light input to the lens, the largest change in polarization is the circular component.

The total polarization of the light input into the lens system is constrained by

$$P_{\text{tot}} = \left(\frac{M}{I}\right)^2 + \left(\frac{C}{I}\right)^2 + \left(\frac{S}{I}\right)^2 \le 1. \tag{9}$$

If the lens only alters the polarization due to changes in birefringence or local reflectance, then P_{tot} will be constant and variations in, for example, circular polarization should be offset by commensurate changes in linear polarization. Taking the total derivative of Eq. (9) and rearranging,

$$\left(\frac{S}{I}\right) d\left(\frac{S}{I}\right) = -\left[\left(\frac{M}{I}\right) d\left(\frac{M}{I}\right) + \left(\frac{C}{I}\right) d\left(\frac{C}{I}\right)\right]. \tag{10}$$

The derivatives are taken to be the change in polarization when the lens is stressed, e.g., $d(C/I) = \langle \Delta C/I \rangle$. The left-hand

Table 2. Total Change in Circular and Linear Polarizations as Defined by Eq. (10) Using Data from Table 1

Lenses	δP	S/I	(C/I)
Thick	-1	$4.1(9)\times10^{-5}$	$-7(5)\times10^{-5}$
Thick	$+1$	$-1.5(2)\times10^{-4}$	$-1.5(6)\times10^{-4}$
Thin	-1	$3.5(2)\times10^{-4}$	$5(2)\times10^{-4}$
Thin	$+1$	$-4.5(2)\times10^{-4}$	$-4(2)\times10^{-4}$

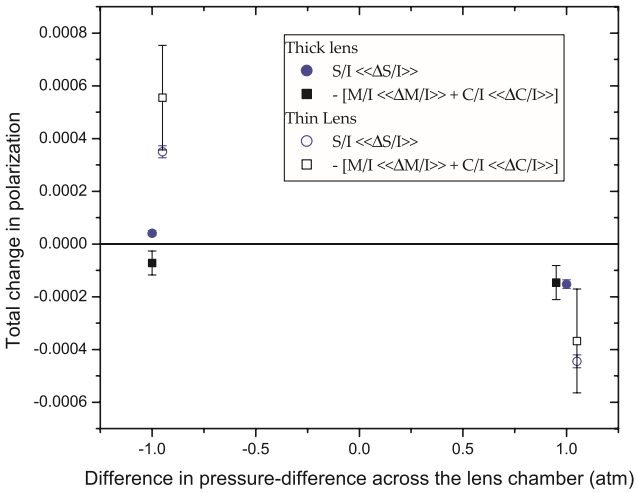

Fig. 8. Total change in the circular polarization and the negative total change in linear polarization observed when the lens is subjected to stress. All data occur at $\delta P = \pm 1$, but are shifted on the abscissa to aid in readability. The change in total linear polarization should have the same magnitude as the total change in circular polarization. The changes are expected to be symmetric about zero when the stress on the lens changes direction.

side of Eq. (10) is now defined as the *total change in circular polarization*, and the right-hand side as the negative *total change in linear polarization*. Using the data presented above, the left- and right-hand sides of Eq. (10) are calculated independently and presented in Table 2, and echoed in Fig. 8. For a given lens and pressure trial, the two right-most columns of Table 2 should be equal if the combined lenses are purely birefringent. Furthermore, the changes are expected to be symmetric about zero when the stress on the lens changes direction. The data show that these statements are generally true, within the systematic uncertainty of the measurements. Finally, these data can be used to estimate a total percentage change in polarization. Considering that the total input polarization is near unity, $P_{\text{tot}} \cong 1$, and using the thin-lens data at $\delta P = +1$ as examples, the stress of 1 atm changed the perceived circular polarization by ~0.05%, with a commensurate change in linear polarization.

5. SIMULATION AND MODELING

At least two effects could contribute to the observed changes in the polarization of light associated with the bulging lenses:

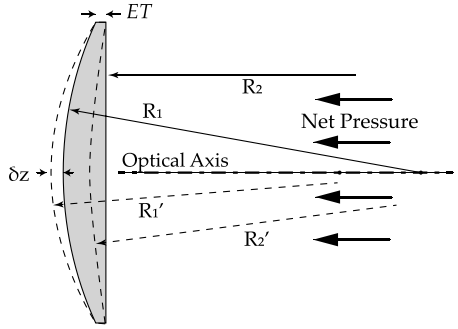

Fig. 9. The assumed change in shape for a plano–convex lens with edge thickness ET. Distances R_1 and R_2 are the radii of curvature for the convex- and plane-side, respectively, when unstressed. When stressed with net pressure difference as shown, the radii of curvature become R_1' and R_2'.

stress-induced birefringence and changes in the Fresnel refraction of light due to the pressure-dependent radii of curvature of the surface of the lenses. The latter effectively changes the angle of incidence of each individual light ray upon the lens. To help isolate and quantify the magnitude of each effect's contribution to the observed changes in polarization, the optomechanical ray-tracing software TracePro was used to model the light source ("A–C") and plano–convex lens ("D") components of the experimental apparatus shown in Fig. 2. Though TracePro does not model the stress of optical components, it can quantify the contribution of the pressure-dependent radii of curvature to the changes in polarization.

When the lens is stressed due to a uniform pressure difference, it is assumed to change shape, as shown in Fig. 9. The radii of curvature for the convex- and plane-side of the lens (R_1 and R_2 respectively) are assumed to change to R_1' and R_2', with the edges of the lens fixed. The displacement of the central portion of the lens δz is estimated using a finite-element analysis (FEA; Autodesk Inventor Pro 2018) with a variety of applied pressures. Our FEA simulation assumed a Young's modulus of 68,000 MPa, a Poisson ratio of 0.19, and a shear modulus of 28,500 MPa. From δz and simple geometry considerations, new radii of curvature were calculated assuming that the surfaces of the lens remain spherical. The Thorlabs LA1725 lens was considered as an example. Figure 10 shows the expected radii of curvature for a variety of applied pressures. These new radii of curvature were used in the TracePro simulations.

In the TracePro simulations, a point source produces light at a wavelength of 656 nm. The light passes through an ideal polarizer with a horizontal pass axis ($M/I = 1$) and is then incident upon a double plano–convex lens collimating system like that shown in Fig. 2 ("D"). The distance between the point source and lens was equal to the focal length of the lens. After passing through the double lens, polarization maps of the cross sections of the transmitted light beams are computed by the program. The plano–convex lenses used in the simulations are the same 50-mm diameter lenses used in the collimating lens system ("D") described above (Edmund #32-974 and Thorlabs LA1725). Using the radii of curvature as determined by FEA, seven different TracePro simulations were conducted for seven different pressure differences: ±4 atm, ±2 atm, ±1 atm, and 0 atm, for a total of 14 simulations for each lens used in the

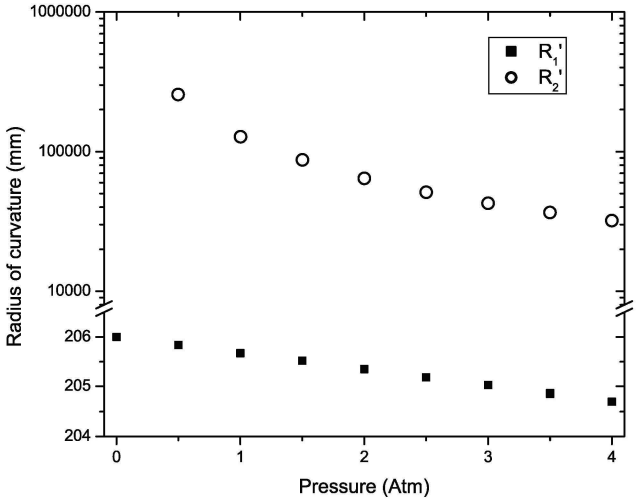

Fig. 10. Calculated radii of curvature of the convex and flat side (R_1' and R_2', respectively) of a Thorlabs LA1725.

experiment. In addition to the two lenses mentioned above, two other lenses with 25-mm diameters and similar focal lengths (Edmund #32-863 and Thorlabs LA1172) were used in single-lens simulations at the same seven pressure differences, for an additional 28 simulations, and 42 in total. The four different lenses used in these simulations have center thicknesses ranging from 2.4 to 9 mm.

One advantage of these simulations is that they can reveal the changes in the polarization in individual parts of the beam cross section, whereas the experiment essentially measures the average polarization across the full cross section. Figure 11 shows typical polarization maps produced by these simulations.

To compare our simulations to experiment, the polarization values are averaged across the face of the lens. For all 48 simulations, the average polarization of the light emerging from the lens is $M/I \cong 1$, $C/I \cong 0$, and $S/I \cong 0$ within 1 part in $\sim 10^6$, which we assume corresponds to the numerical accuracy of the integrated average, since the results did not depend on pressure. This suggests that changes in the radii of curvature of the lens surfaces, and the corresponding changes in the transmitted light due to Fresnel's equations, are an insignificant contributor to polarization changes. Thus, the polarization variations observed must be due to stress-induced birefringence.

We note also from Fig. 11 that the lens's circular symmetry further reduces any change in the integrated average of the Stokes parameters due to lens bulge. Not only are the local changes in C/I and S/I small, but they average to zero azimuthally. The requirement that P_{tot} not change due to transmission through the lens means that the local production of nonzero values of C/I and S/I must reduce the value of M/I in these lens regions. Thus, a net change in the integrated M/I can be expected, although, as we indicated above, the modeling of our experiment in TracePro indicates that it is immeasurably small.

We now consider stress-induced birefringence and its effect on the transmitted Stokes parameters. When a uniaxial normal stress is applied to a sample of glass, it possible to have two different indices of refraction, $n_\perp$ and $n_\parallel$, corresponding to light

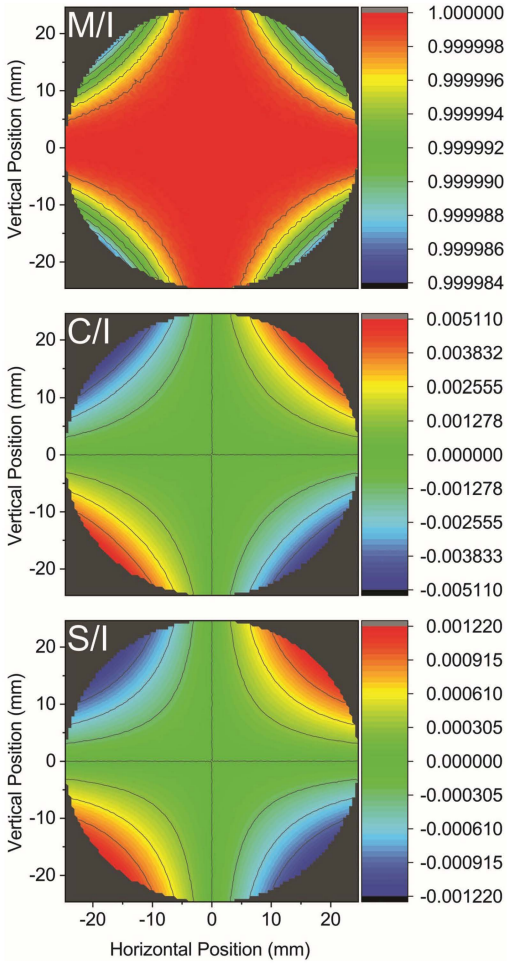

Fig. 11. Typical beam cross sections for M/I, C/I, and S/I of initially horizontally linear-polarized light after passing through the 50mm diameter lens with a center thickness of 9 mm (Edmund #32-974) at a pressure difference of +4 atm. The propagation direction of the beam is into the page. These maps are characteristic of all the simulations.

propagating through the sample with electric vector perpendicular or parallel to the applied stress. The nonzero difference $n_\perp - n_\parallel$ will lead to a relative phase shift between the two electric vectors. According to the stress-optic law [19], the relative phase difference is determined from

$$\delta = \frac{2\pi t}{\lambda} C\,(\sigma_1 - \sigma_2)\,, \tag{11}$$

in which t is the thickness of the sample, λ is the wavelength of light, C is the stress-optic coefficient for the material, and $\sigma_{1(2)}$ is the first (second) principle stress. Stresses are estimated, again using FEA, for both the Edmund #32-974 and the Thorlabs LA1172 lenses with an applied pressure of 1 atm following the orientation given in Fig. 9. While $\sigma_1 - \sigma_2$ must be strictly zero at the center of the lens, the value of σ_1 on the optical axis and on the convex surface is used as a convenient, representative value for placing an upper limit estimate on the phase difference, since we know the thickness t at this point. Using $C \sim 3 \times 10^{-13}$ fringes/(dyne/cm^2) [20], and the taking the thickness to be the center thickness for the appropriate lens,

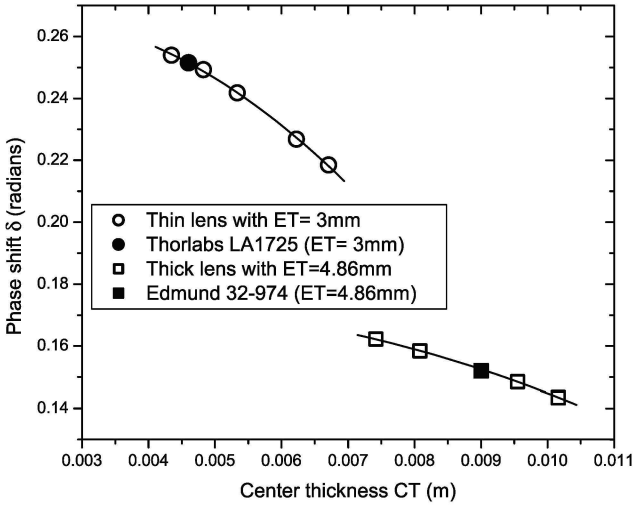

Fig. 12. Calculated phase difference δ [Eq. (11)] for lenses similar to Thorlabs LA1725 with edge thickness $ET = 3$ mm and for lenses similar to Edmund 32-974 with $ET = 4.86$ mm.

the local upper limit of the phase shift δ is calculated for these lenses and presented in Fig. 12. A family of phase difference data is also calculated by adjusting the center thickness of each lens while keeping the edge thickness constant. This also means that the radii of curvature of the lenses have changed. The data in Fig. 12 suggest that a thinner lens will be more susceptible to stress-induced birefringence.

Equation (11) and the simulation data suggest that local birefringence can be introduced in our lenses with 1 atm of pressure. However, with the uniform pressure applied to the face of the lens, the stress pattern is axially symmetric about the optical axis. Even if a local region on the lens produces a phase shift with a given input linear polarization, there will be a commensurate phase change of opposite sign on the opposite side of the optical axis. Thus, in a manner consistent with our symmetry considerations for the TracePro calculations discussed above, the integrated average birefringent phase shift of a perfectly symmetric *ideal* lens will be zero. In other words, the lens could not produce circular polarization with any input linear polarization.

Assuming now that the lens is imperfect and has some effective pressure-dependent retardance δ' as before, we can estimate the change in retardance $d\delta'$ and effective fast axis β' from Eq. (7). For example, using all measured data for the thin lens (Table 1), the average input polarization (given above), and all algebraic pathways available in Eq. (7), we determine an average $\beta' = -12°$ and $d\delta' = +0.0067(8)$ rad for the $\delta P = +1$ atm data and $d\delta' = -0.0063(6)$ rad for the $\delta P = -1$ atm data. This phase difference is ~2.5% of the maximum phase change calculated above and can be explained by random variations throughout the bulk of the lens.

6. CONCLUSIONS

The ultimate accuracy of a noble gas electron polarimeter will depend on the accuracy by which light polarization can be measured. The effects of atmospheric stress on a light-collection lens and how this can alter polarization has been demonstrated. Our light-source intensity, lens system, and optical polarimeter approximates the situation found in a typical atomic physics experiment. We have demonstrated that a pressure difference of 1 atm on a lens will alter the perceived polarization by as much as 0.05% with typical borosilicate lenses. This effect was demonstrated to change signs when the direction of the stress is reversed, and scale with the thickness of the lens.

We examined two possible sources of this effect in an effort to predict scaling with lens thickness. In the ideal situation, both the stress-induced birefringence and the changes produced by Fresnel refraction are symmetric about the optical axis. That is to say, the two effects cannot exhibit a sense of rotation, so it is impossible to produce nonzero S/I from a linear input polarization. In other words, by symmetry, there cannot be an integrated phase difference introduced by an ideal lens. Stress-induced birefringence can only arise from a lens with microscopic defects and asymmetries introduced by the manufacturing process. Such stress-induced birefringence will not be identical for any two components, even if they do share the same manufacturer's part number. One can assume, however, that both the thick and thin lens have similar distributions of random variations in the bulk. Then, broadly generalizing the results presented in Fig. 12, the thinner lens will have more susceptible stress-induced birefringence for similar applied pressures.

Funding. National Science Foundation (PHY-1632778, PHY-1806771).

Acknowledgment. The use of TracePro in this work was made possible by an academic license supplied by Lambda Research Corporation. The authors thank Lambda Research Corporation for its support. The use of Autodesk Inventor Pro (2018) was made possible by an educational license.

Disclosures. The authors declare no conflicts of interest.

REFERENCES

1. E. Chudakov, "Precision electron polarimetry," AIP Conf. Proc. **1563**, 29–36 (2013) and references therein.
2. T. J. Gay and F. B. Dunning, "Mott electron polarimetry," Rev. Sci. Instrum. **63**, 1635–1649 (1992).
3. X. Roca-Maza, "Theoretical calculations for precision polarimetry based on mott scattering," Europhys. Lett. **120**, 33002 (2017).
4. K. Foreman and T. J. Gay, "Accurate electron spin optical polarimetry (AESOP)," Bull. Am. Phys. Soc. **63**(5), 56 (2018).
5. P. S. Farago and J. S. Wykes, "Optical detection of electron polarization," J. Phys. B **2**, 747–756 (1969).
6. J. S. Wykes, "A general optical detector of the polarization of low energy electrons," J. Phys. B **4**, L91–L94 (1971).
7. T. J. Gay, J. E. Furst, K. W. Trantham, and W. M. K. P. Wijayaratna, "Optical electron polarimetry with heavy noble gases," Phys. Rev. A **53**, 1623–1629 (1996), and references therein.
8. K. Blum, *Density Matrix Theory and Applications*, 2nd ed. (Plenum, 1996), pp. 32–37.
9. K. Bartschat and K. Blum, "Theory and physical importance of integrated state multipoles," Z. Phys. A **304**, 85–88 (1982).
10. B. G. Birdsey, H. M. Al-Khateeb, M. E. Johnston, T. C. Bowen, T. J. Gay, V. Zeman, and K. Bartschat, "Near-threshold measurement of integrated stokes parameters for Kr excited by polarized electrons," Phys. Rev. A **60**, 1046–1052 (1999).
11. M. Pirbhai, D. M. Ryan, G. Richards, and T. J. Gay, "Compact inline optical electron polarimeter," Rev. Sci. Instrum. **84**, 053113 (2013).

12. A. Steffen, W. Alt, M. Genske, D. Meschede, C. Robens, and A. Alberti, "Note: In situ measurement of vacuum window birefringence by atomic spectroscopy," Rev. Sci. Instrum. **84**, 126103 (2013).
13. B. K. Park, A. O. Sushkov, and D. Budker, "Precision polarimetry with real-time mitigation of optical-window birefringence," Rev. Sci. Instrum. **79**, 013108 (2008).
14. M. Shribak, S. Inoue, and R. Oldenbourg, "Polarization aberrations caused by differential transmission and phase shift in high-numerical-aperture lenses: Theory, measurement, and rectification," Opt. Eng. **41**, 943–954 (2002).
15. K. W. Trantham, "An in vacuo precision optical polarimeter," Rev. Sci. Instrum. (to be published).
16. H. G. Berry, G. Gabrielse, and A. E. Livingston, "Measurement of the Stokes parameters of light," Appl. Opt. **16**, 3200–3205 (1977).
17. J. W. Maseberg and T. J. Gay, "Fluorescence polarization of helium negative-ion resonances excited by polarized electron impact," J. Phys. B **39**, 4861–4870 (2006).
18. J. R. Taylor, *An Introduction to Error Analysis: The Study of Uncertainties in Physics Measurements*, 2nd ed. (University Science Books, 1997), Chap. 7.
19. J. W. Dally and W. F. Riley, *Experimental Stress Analysis*, 3rd ed. (McGraw-Hill, 1991).
20. K. Schwertz, "Useful estimations and rules of thumb in optomechanics," MS Report (University of Arizona, 2010).